EurJOC
European Journal of Organic Chemistry

Research Article
doi.org/10.1002/ejoc.202201301

Chemistry Europe
European Chemical Societies Publishing

www.eurjoc.org

Special Collection

# Synthesis of [60]Fullerene Hybrids Endowed with Steroids and Monosaccharides: Theoretical Underpinning as Promising anti-SARS-CoV-2 Agents

Reinier Lemos,[a] Kamil Makowski,[b] Luis Almagro,[a] Blanca Tolón,[c] Hortensia Rodríguez,[d] M. Ángeles Herranz,[e] Dolores Molero,[f] Nazario Martín,*[e] and Margarita Suárez*[a]

Cyclopropanation reactions between $C_{60}$ and different malonates decorated with monosaccharides and steroids using the Bingel-Hirsch methodology have allowed the obtention of a new family of hybrid compounds in good yields. A complete set of instrumental techniques has allowed us to fully characterize the hybrid derivatives and to determine the chemical structure of monocycloadducts. Besides, the proposed structures were investigated by cyclic voltammetry, which evidenced the exclusive reductive pattern of fullerene Bingel-type monoadducts. Theoretical calculations at the DFT-D3(BJ)/PBE 6-311G(d,p) level of the synthesized conjugates predict the most stable conformation and determine the factors that control the hybrid molecules' geometry. Some parameters such as polarity, lipophilicity, polar surface area, hydrophilicity index, and solvent-accessible surface area were also estimated, predicting its potential permeability and capability as cell membrane penetrators. Additionally, a molecular docking simulation has been carried out using the main protease of SARS-CoV-2 (Mpro) as the receptor, thus paving the way to study the potential application of these hybrids in biomedicine.

## Introduction

Fullerenes are among the most exciting molecules discovered last century by Kroto et al.[1] Many research groups have been devoted to studying their reactivity, photophysical and electrochemical properties, and the possible use of their derivatives, both in materials science[2] and in biomedical applications.[3] Among the various potential applications that fullerene derivatives possess, their use in medicinal chemistry is probably one of the most promising and striking at the time. They have shown some biological properties, both in vitro and in vivo, to be used for medical purposes.[4] The ability of $C_{60}$ and its derivatives to capture a large number of radicals per molecule makes them potentially useful drugs for preventing or treatment pathologies involving oxidative processes, such as cardiovascular[5] or degenerative diseases.[6] Also, fullerenes have been used as HIV-1 protease inhibitors,[7] in photodynamic therapies,[8] as antioxidant agents,[9] as emerging tool for cancer treatment,[10] and as antiviral agents.[11]

Although, one of the most significant applications of fullerenes is its potential use in biological systems, an obstacle to its application is the lack of solubility in water and the low solubility in most organic solvents.[12] The chemical modification of [60]fullerene to increase its solubility, can also lead to the formation of conjugates with different physicochemical properties, thus increasing the applications of this allotrope of carbon.[13]

Among the many reactions experienced by fullerenes,[14] the cyclopropanation reaction forming a variety of stable derivative in which a three-membered ring is fused to the fullerene, represents one of the most efficient alternatives for functionalizing these carbon allotropes. Traditionally, this reaction uses an intramolecular halide shift using a malonic acid derivative.[15] In

[a] R. Lemos, Dr. L. Almagro, Prof. Dr. M. Suárez
Laboratorio de Síntesis Orgánica
Facultad de Química
Universidad de la Habana
10400-La Habana (Cuba)
E-mail: msuarez@fq.uh.cu
[b] Dr. K. Makowski
Department of Surfactants and Nanobiotechnology
Institute for Advanced Chemistry of Catalonia. (IQAC-CSIC), 08034-Barcelona (Spain)
and
Centro de Investigación Biomédica en Red Bioingeniería
Biomateriales y Nanomedicina (CIBER-BBN)
28029-Madrid (Spain)
[c] Dr. B. Tolón
Finlay Vaccines Institute
Havana, 10600-La Habana (Cuba)
[d] Dr. H. Rodríguez
Yachay Tech University
School of Chemical Sciences and Engineering Urcuqui, 100119-Urququi (Ecuador)
[e] Dr. M. Á. Herranz, Prof. Dr. N. Martín
Departamento de Química Orgánica
Facultad de Ciencias Químicas
Universidad Complutense de Madrid
28040-Madrid (Spain)
E-mail: nazmar@quim.ucm.es
https:nazariomartingroup.com
[f] Dr. D. Molero
CAI RMN Universidad Complutense de Madrid
28040-Madrid (Spain)

Supporting information for this article is available on the WWW under https://doi.org/10.1002/ejoc.202201301

Special Collection Part of the "Organic and Supramolecular Chemistry in Latin America" Special Collection.

this way, different ligands can be introduced by prior functionalization with malonate linkers[16] following the Bingel-Hirsch methodology.[17] Then, the cyclization occurs by direct treatment of $C_{60}$ with malonates in the presence of carbon tetrabromide ($CBr_4$) and 1,8-diazabicyclo[5.4.0]undec-7-ene (DBU), using the above-mentioned procedure. Under these conditions, the reaction occurred smoothly even at room temperature. However, these methanofullerenes can undergo under the appropriate conditions a retrocyclization reaction and, therefore, caution must be exercised when handling the products.[18]

In the search for fullerene derivatives that could present a greater solubility in biological media to be used in biomedicine, our research groups have developed the synthesis of several fullerene hybrids with potential use in medicinal chemistry. In that sense, employing the Prato methodology,[19] our group has reported the synthesis and characterization of novel hybrid systems based on fullerenes with different molecules such as heterocycles[20] and steroids.[21]

Also, using the Bingel-Hirsh reaction we carried out the conjugation of [60]fullerene with naturally occurring steroids such as cholesterol,[22] epiandrosterone,[23] and dehydroepiandrosterone[24] with relevant biological properties. Recently, we reported the synthesis of hybrids of dehydroepiandrosterone conjugated to $H_2@C_{60}$ and $C_{60}$ by means of a malonate bridge.[25] The molecular interaction of these compounds with the HIV-1[26] and SARS-CoV-2 proteases[27,28] as receptors, open the door for the potential application of these structures in biomedicine as antivirals agents. Moreover, theoretical studies were conducted on these fullerene steroid conjugates to determine the factors that control the geometry of these hybrid molecules. The morphology and particle size in aqueous solution were determined by transmission electron microscopy.[29] A review containing the work developed in this field by our research groups has recently been published.[30]

On the other hand, incorporating carbohydrates into hybrid systems is being used for their ability to interact with lectins on the cell surface, and for their participation in biological processes such as cell growth and differentiation.[31] Due to these characteristics, they have been covalently linked to [60]fullerene, and the conjugates obtained tested as agents against bacterial and viral infections.[32] Martin et al. reported the synthesis of multivalent glycofullerenes contained 120 mannoses and up to 360 disaccarides, which act as potent inhibitors of a model of the Ebola virus as well as other emergent viruses like Zika and Dengue.[33] Tanimoto et al. synthesized a derivative of $C_{60}$ linked to a glucose unit that degrades the HIV-1 protease under irradiation without additives, causing a decrease in the number of cells infected with HIV-1 according to in vitro assays.[34]

Taking into account our expertise using the cyclopropanation reaction to obtain a variety of mono[22,23] and bis-steroidal[24] methanofullerenes, and following our interest in the chemistry of fullerene hybrids, we have decided to increase the structural diversity in these families of compounds. Thus, the presence of molecules such as monosaccharides[35] and steroids[36] in the hybrids, could increase their affinity for biological receptors and hence their potential use in medicinal chemistry. Therefore, herein, we describe the synthetic methodology to obtain new fullerene hybrids containing monosaccharide and steroid moieties based on the Bingel-Hirsch reaction.[17] First, it was necessary to develop a methodology to obtain malonates with bioactive moieties as sugars and steroids and add the bioactive conjugates to [60]fullerene. The use of monosaccharides such as D-galactose, D-mannose, and L-rhamnose has been related with the increase of the hybrids solubility and their use to allow greater recognition in the biological environment. On the other hand, diosgenin and cholesterol scaffolds in the conjugates will enable them to penetrate cell membranes and interact with specific hormonal receptors.

In agreement with the previous results obtained in our group related to the synthesis of [60]fullerene hybrids, in this work, we report the synthesis of novel steroid-monosaccharidemethanofullerenes with potential biological applications. In addition, the electrochemical properties, thermal stability, deep structural analysis, and chemical-physical properties were studied through theoretical calculations. Besides, molecular docking was carried out prior optimization of the structures by the theoretical DFT-PBE method and 6–311G(d,p) basis set, to estimate the potential application of the hybrids as HIV-1 protease inhibitors. Some stereoelectronic parameters were calculated to determine the electronic interactions present in these hybrid molecules.

## Results and Discussion

New hybrid compounds were prepared using the Bingel-Hirsch protocol in a multistep synthetic procedure (see Scheme 1).

In contrast to the methods previously reported by the group[22–24] for obtaining alkyl malonylsteroid derivatives, in this paper Meldrum's acid was employed as precursor. Therefore, the first step was the preparation of the required starting malonates by treatment of two different sterols – diosgenin (**1a**) and cholesterol (**1b**) – with commercially available Meldrum's acid through acyl nucleophilic substitution, to obtain a new steroidal acid **2a** and **2b**. The reaction was carried out at 110 °C, allowing the Meldrum's acid ring to open. The products were purified by column chromatography, using a *n*-hexane/ethyl acetate (1 : 1) mixture as the eluent. In this way, two novel steroidal 3-oxopropanoic acids (**2a** and **2b**) were obtained in 85 % and 86 %, respectively.

The structure of the steroidal malonates was verified by spectroscopic techniques ($^1$H and $^{13}$C NMR), mass spectrometry, and elemental analysis (see Experimental Section and Supporting Information). The formation of steroidal acids **2a** and **2b** was pointed out by the presence of the methylene protons of malonate in the $^1$H NMR spectra, which appeared as singlets near 3.40 ppm. In addition, the signals from H3 (~4.70 ppm) are unshielded compared to the same proton signal in the starting steroids (~4.30 ppm) confirming the functionalization of the hydroxyl attached to C3. In addition, two signals appear at ~169 and ~167 ppm in the $^{13}$C NMR spectra, assignable to the malonate carbonyl groups. The unshielded signal of C3 (~

Research Article
doi.org/10.1002/ejoc.202201301



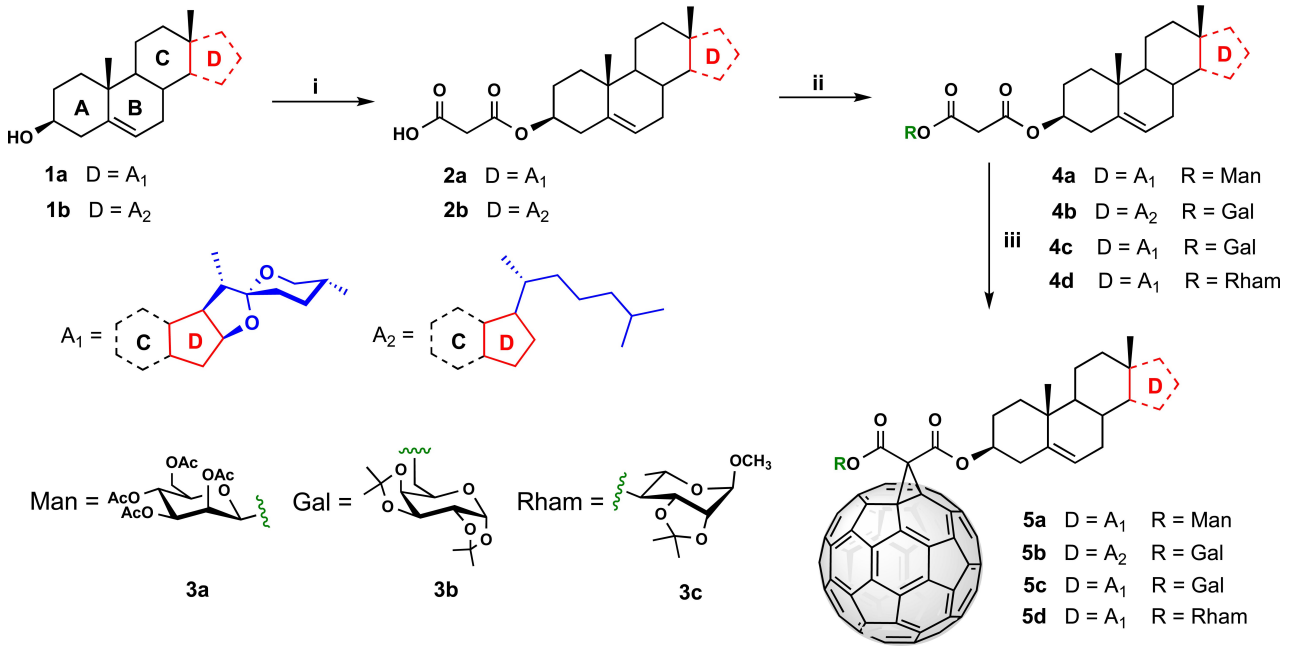


**Scheme 1.** Synthesis of hybrid monosaccharide-steroid-fullerene (**5a**–**5d**). (i) Meldrum's acid, toluene, reflux, (ii) monosaccharide (**3a**, **3b** or **3c**), $BF_3{\cdot}Et_2O$ or EDC, DCM dry, 1 h, (iii) $C_{60}$, DBU, $CBr_4$, toluene, room temperature.

77 ppm) relative to the chemical shift of C3 in the starting steroids (~73 ppm) is due to the functionalization of the hydroxyl group.

It is known that sugars have important biological functions in cell recognition, transport and cell adhesion, increasing the biocompatibility of the scaffolds connected to them and generating glycoconjugates with high affinity for cell receptors.[31] Taking this background into account, an important part of the work was the previous functionalization of some monosaccharides such as D-mannose, D-galactose and L-rhamnose to subsequently conjugate them to steroidal malonates. The hydroxyl groups of monosaccharides have a similar nucleophilic reactivity and should be selectively protected to achieve good yields in conjugation reactions with malonyl steroids. The saccharide fragments were conveniently functionalized in different positions and thus achieved different binding sites to evaluate the potential activity of the glycoconjugates, and the viability during the conjugation to the steroidal fragment.

The conjugation of the monosaccharides **3a**, **3b** or **3c** to the steroidal acids **2a** and **2b** was carried out using two synthetic methods, taking into account the positions where the sugar is linked and their reactivity. The monosaccharides were linked at the anomeric position and at the C4 and C6 carbons. The glycosylation reaction occurs through a nucleophilic substitution in the anomeric carbon, favored by the activating character of the trichloroacetoimidate group. The glycosidic bond is formed between the monosaccharide (donor) and the steroid through the spacer malonate to generate malonates **4a**.[37] Conjugates **4b**–**4d** are obtained by an esterification reaction using EDC as activating of the carboxyl group.[38]

In both cases, the reactions took place in one hour, and the reaction crudes were purified by column chromatography. In this way, four new malonyl-substituted steroids (**4a**–**4d**) were obtained with yields ranging between 60–75%. As the malonate group fragment of the steroidal acids is the only one involved in the reaction, it can be deduced that the different sugars' structure directly influences the reaction yield. Although the reactions yields are similar, the lowest yield value corresponds to conjugate **4a**. This experimental result could be explained considering that the presence in D-mannose of an axial acetate group linked to C2 causes a steric hindrance in the β face against the approximation of the steroidal acid to the anomeric position. In the other conjugates, there is less steric hindrance in the different conjugation positions.

The structures of compounds **4a**–**d** were verified using spectroscopic techniques ($^1$H and $^{13}$C NMR), mass spectrometry and elemental analysis (see Experimental Section and Supporting Information). The methylene protons of the malonates were observed as singlets at ~3.40 ppm in the $^1$H NMR spectra. The proton H1′ of conjugate **4a** has a $J = 1.9$ Hz, which indicates a weak coupling with its neighboring proton H2′ due to its *cis* disposition. On the other hand, the $^{13}$C NMR shows two signals at ~165 ppm corresponding to the carbonyl carbons of the malonate group, showing that this group remains in the structure without modifications. The carbon signals corresponding to the functionalized positions during the conjugate formation are more unshielded related to the starting monosaccharides due to the strong unshielding effect of the carboxyl group of the malonate.

Finally, the [60]fullerene functionalization was performed by using the Bingel-Hirsch reaction conditions. For this, the $C_{60}$ and

the steroidal malonate (**4a**–**4d**) were dissolved at room temperature in toluene and in the presence of carbon tetrabromide as the halogenating agent and DBU as the base, the corresponding methano[60]fullerene was generated. The formation of the monoadducts occurs with a color change from purple to brown in the reaction mixture. The reaction was stopped after two hours when the formation of more polar species than the monoadduct were observed by TLC (polyadducts). Purification was performed by flash chromatography, where carbon disulfide was first used to separate the $C_{60}$ that remained unreacted and subsequently the monoadduct was eluted with dichloromethane. After purifying the different reaction crudes, the corresponding methano[60]fullerenes **5a**–**5d**, were obtained as stable brown solids, with 63–65% yields. These values are according to those previously obtained for steroid-fullerene hybrids.[22–24]

The HPLC profiles of the reaction mixtures (toluene/acetonitrile 9:1; 1 mL/min) show peaks at 5.3, 5.2, 5.6 or 4.0 min, corresponding to **5a**, **5b**, **5c**, and **5d**, respectively (see Supporting Information S72-S76). The peak with the highest retention time on each chromatogram corresponded to unreacted $C_{60}$ and other minor peaks attributed to $C_{60}$ epoxide and the formation of polyadducts were also observed.

The structural elucidation of the carbohydrate-steroid-fullerenes (**5a**–**5d**) was accomplished using different spectroscopic techniques (see Experimental Section and Supporting Information). $^1$H NMR spectroscopy reveals the presence of the disubstituted malonates covalently linked to the [60]fullerene. No signal corresponding to the methylene protons of the starting malonates (**4a**–**4d**) at ~3.38 ppm was identified, indicating the functionalization of this spacer. The presence of $C_{60}$ modifies the chemical shifts of the atoms close to its surface, and, particularly, those of the monosaccharide protons, which appear more unshielded. The proton H3 of the ring A resonates at ~5.00 ppm compared to the signal of the same proton (~4.65 ppm) in **4a**–**4d**. On the other hand, the $^{13}$C NMR spectrum shows an increase in the number of signals in the $sp^2$ carbon region corresponding to $C_{60}$. The three signals from the $sp^3$ carbon atoms of the cyclopropanes ring were observed, two at ~72 ppm and the other at ~52 ppm. Furthermore, two signals assignable to the carbonyl carbons of the malonate group appear at ~162.8 and ~168.9 ppm. The position of the signals of the steroid and carbohydrate backbones did not show significant variation. The analysis of the 2D NMR spectra has allowed the unambiguous assignment of the signals of the $^1$H and $^{13}$C NMR spectra straightforwardly.

The structure of the monoadducts obtained was confirmed by high-resolution mass spectrometry using the MALDI-TOF technique. For all the compounds, a peak with an *m/z* ratio equal to the protonated or deprotonated molecular ion is observed, with the exception of hybrid **5d**, which shows a peak corresponding to the molecular ion $[M]^{\bullet+}$ (See Experimental and Supporting Information).

UV-Vis spectroscopy is important to corroborate the formation of [6,6]-closed fullerene adducts. The four synthesized hybrids presented a weak absorption band center at 430 nm, characteristic of [60]fullerene monoadducts,[39] see Figure S71 in the Supporting Information. Also, the FTIR spectra exhibited the specific band of organofullerene derivatives at ca. 730 $cm^{-1}$[40] and a signal at 1740 $cm^{-1}$ corresponding to the C=O stretching vibration (see Supporting Information).

The hydrolysis of monosaccharide's protecting groups could increase the fullerene derivatives' polarity. The isopropyliden group is more stable than the acetate group in biological media, because the acetyl esterase can hydrolyze the last one.[41] Because of the presence of isopropiliden moiety, **5d** was chosen as a model molecule to test the removal of the protecting group. Hydroxyl groups deprotection in **5d** was achieved with trifluoroacetic acid[42] affording **6** in 35% yields (see Scheme 2).

The structure of hybrid **6** was confirmed by $^1$H- and $^{13}$C NMR spectroscopic techniques, and high-resolution mass spectrometry (see Experimental Section and Supporting Information). In the most unshielded region of the spectrum, the characteristic signals of the steroidal skeleton are located, namely the multiplet at 5.48 ppm assignable to H6 (ring B) and the multiplet at 5.04 ppm to H3 (ring A). The only protective group removed was isopropylidene, since the singlets of the methyl groups were found at 1.65 and 1.37 ppm in the spectrum of **5d** disappeared. In addition, two signals corresponding to two hydroxyl groups, which were not present in the starting hybrid, were observed at 3.09 and 2.50 ppm groups were observed at 3.09 and 2.50 ppm. The other signals of **6** did not show significant variation concerning those identified for compound **5d**. (See Experimental and Supporting Information).

Although the solubility of these hybrids was not experimentally determined, it was found that the conjugation of steroids and monosaccharides to $C_{60}$ improves the solubility of the hybrid compounds in organic solvents such as chloroform, dichloromethane, and dimethylformamide, among others. In the case of compound **6**, it becomes slightly soluble in water after ultrasonication. A fact that could enable further biological investigations.

For a better understanding of molecular interactions and properties, quantum calculations were performed. After building the 3D structures of compounds **5a**–**5d** first semi-empirical extended tight-binding method was used, namely GFN2-xTB.[43] This method is a second and very recent version of the tight-binding method from Grimme laboratory[44] with several parametrizations, including D4 dispersion model and presents some advantages over previously used by us PM6 semi-empirical[45] as better approximations of bond length and improved non covalent interaction energies. This more robust method is still swift, and we used it for pre-optimization and starting point in DFT optimizations[46] of all molecules. For more accurate, but

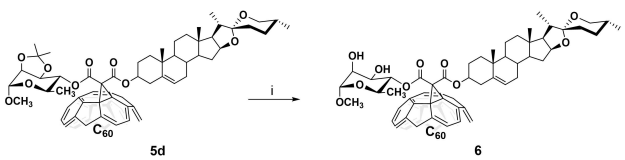


**Scheme 2.** Selective deprotection. (i) $CF_3CO_2H$, $H_2O$, $CHCl_3$, r.t., 14 h.

Research Article
doi.org/10.1002/ejoc.202201301


computationally expensive DFT calculation, we chose PBE[47] functional as it presents good consensus regarding results and computational demand in big systems such as fullerene derivatives. We also have used dispersion correction D3(BJ)[48] as it significantly improves optimization in medium and big systems. In the first iteration, we optimized structures at double zeta 6-31G(d) and then refined using triple zeta 6-311G(d,p) level[49] of theory for full optimization. The optimized structures were confirmed by lacking imaginary frequencies.

The optimized structures are shown in Figure 1. The previous studies where only a steroid moiety was present showed that the carbonyl groups of the malonic moiety present *s*-trans disposition.[23,24] Herein, where a saccharide moiety is also part of the structure, this tendency is lost. Only in compounds **5a** and **6** are the carbonyls pointing in opposite directions with torsion O=C···C=O angles of −171.67° and −116.04°, respectively. Compounds **5b** and **5c** showed rather synclinal, or close to synclinal in the case of **5d**, predisposition with torsion angles: 65.45°, 78.85° and −96.82°, respectively, were predicted.

The high content of oxygen atoms in monosaccharide or monosaccharide derivatives moieties and the space constraint produced by the fullerene cage might make possible interactions between carbohydrate and steroid moieties. The DFT calculation predicts two interactions of this kind in compound **5a**. The oxygen from the pyran ring from galactose interacts with one of the hydrogen attached to C19 in the methyl group from diosgenin with a distance of 2.536 Å. Also, the oxygen in the carbonyl group located on the acetyl group close to C6′ interact with H4 at 2.525 Å distance. Additionally, the methyl group from the same acetyl group produces a hydrogen bond with the oxygen from the more distant carbonyl group from malonic moiety and the same oxygen seems to interact with H3 (2.493 Å). The absence of carbonyl groups in the galactose of compound **5b** also results in no direct interaction between the cholesterol and galactose scaffolds. However, one of the malonic carbonyl groups interacts with both moieties H6′ (2.309 Å) from the saccharide and H2 (2.758 Å) and H1 (2.763 Å) from cholesterol. In compound **5c** we can observe a weak interaction between the saccharide's oxygen attached to C4 with the hydrogen from methyl C19 from diosgenin (2.603 Å). Another hydrogen bond interaction in this compound stems from the malonic part of the molecule. The closest carbonyl groups interact on the one hand with H3 from the steroid and on the other hand with saccharide H6′ (2.382 Å) and simultaneously with the hydrogen from one of the methyl group close to acetal moiety and C4′ (2.573 Å). Oxygen from pyran ring in compound **6**, similar to compound **5a**, acts as an electron

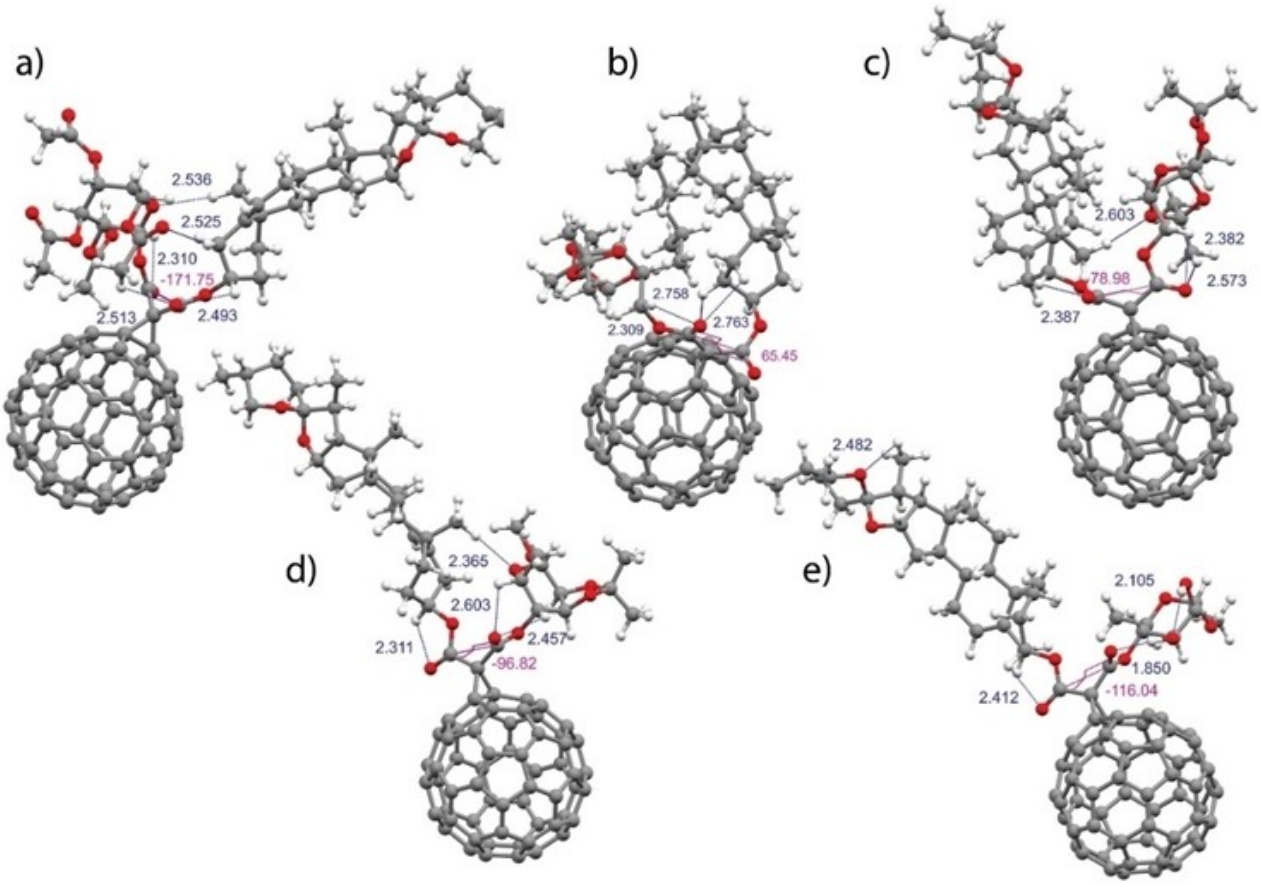


**Figure 1.** Optimized structures of compounds **5a** (a), **5b** (b), **5c** (c), **5d** (d), and **6** (e) using DFT-D3(BJ) at PBE/6-311G(d,p) level of theory. Torsion angles (°) are shown in violet and distances in blue (Å).

Research Article
doi.org/10.1002/ejoc.202201301


donor to H4 from diosgenin (2.229 Å), producing interaction between the two moieties.

Other interactions are due to carbonyl groups from the malonic linker, which in a similar way to compound **5c**, produces hydrogen bonds with the closer moiety. The H3 from steroid ring A interacts with the closest carbonyl (2.311 Å), and the other carbonyl interacts with H4′ (2.457 Å) and 5H′ (2.603 Å) both from saccharide moiety. Compound **6** does not show a direct interaction between the saccharide and the steroid parts. However, another interesting interaction is present in this compound. In this case, rhamnose contributes with free hydroxyl groups making strong hydrogen bonding possible. The hydroxyl group at H2′ interacts with the H from another hydroxyl group at C3′ with OH···O 2.105 Å. However, this hydroxyl group at C3′ forms another and stronger (1.850 Å) hydrogen bond with the closer carbonyl from malonic moiety. The same carbonyl interacts simultaneously with H4′ (2.559 Å). Another malonic carbonyl group interacts with H3 as in previous compounds containing diosgenin steroid with a 2.412 Å distance.

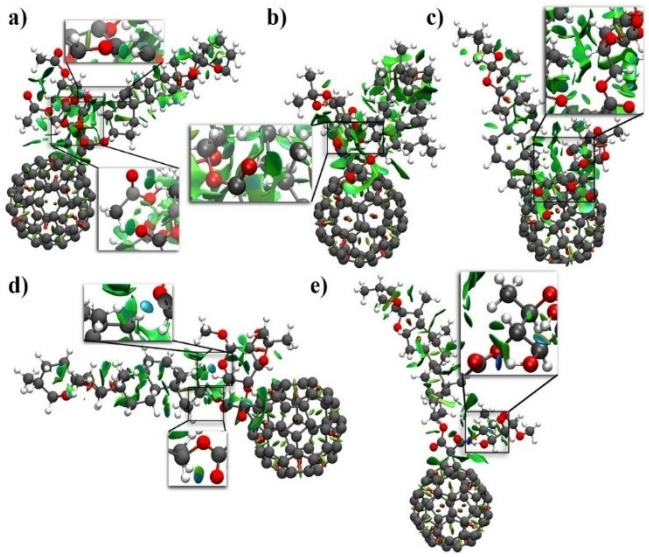


**Figure 2.** Non-covalent interactions of molecules of **5a** (a), **5b** (b), **5c** (c), **5d** (d), and **6** (e). The most important interactions between steroid and sugar moieties are shown as amplification of the zone in each molecule. The isosurfaces with blue color represent strong attractions, green weak attraction forces and red repulsions.

The visual representation of those interactions is shown in Figure 2. The aforementioned interactions between the steroid and the saccharide moieties in optimized compounds are shown as an amplification of the specific zones for a better visualization. The strongest attractive interactions as hydrogen bond where oxygen is an electron donor are represented by blue color, weak interactions by green and in red repulsive interactions. Interestingly, all studied compound show weak interactions between the fullerene and the oxygen atoms from the malonate moieties, represented by relatively big isosurface values. In the cases of compounds **5a**, **5d** and **6**, the oxygen atoms from the saccharides also contributes to those interactions. Additionally, methyl groups from the saccharide moieties in **5a** and **5c** and steroid in **5b** also showed weak attractions to the fullerene.

On the other hand, from the representation of the molecular orbitals in Figure 3, the LUMO orbitals can be observed exclusively in the fullerene nucleus for all the hybrids.

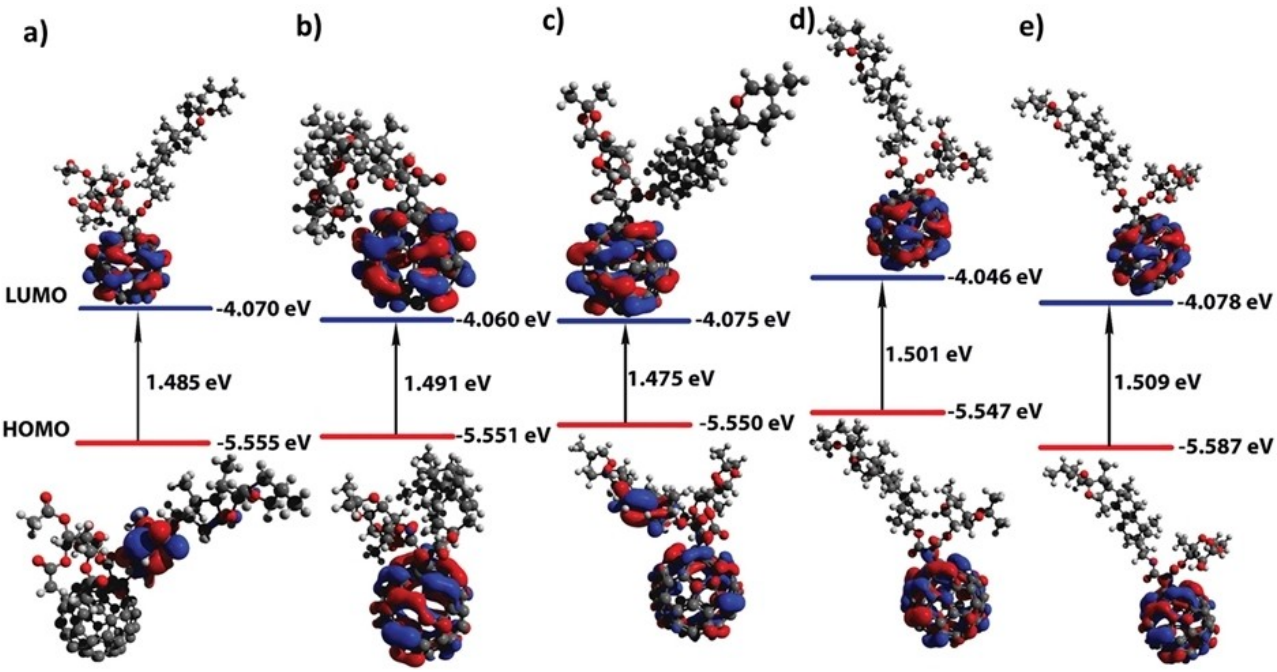


**Figure 3.** Molecular orbitals involved in the transitions HOMO-LUMO of **5a** (a), **5b** (b), **5c** (c), **5d** (d), and **6** (e) calculated using DFT-D3(BJ) method at PBE/6-311G(d,p) level of theory in the gas phase.

Research Article
doi.org/10.1002/ejoc.202201301


In contrast, the electron density of HOMO is located in the steroid skeleton at **5a**, while at **5b**, **5d**, and **6** it is found in the fullerene unit. In a particular case, the HOMO of **5c** is distributed both in the steroid and in the fullerene. In this family of hybrids, similar energies were found for HOMOs and LUMOs, exhibiting an energy gap between them of 1.5 eV.

The surface electronic densities for each hybrid were determined to evaluate the intramolecular interactions. Thereby, the electrostatic potential maps were obtained, which are shown in Figure 4.

The covalent binding of functionalized malonates to fullerene modifies the electrostatic potential distribution in three well-defined regions. In this sense, the negative potential, represented by the red color, was mainly associated with the oxygen atoms belonging to the carbonyl, ester and ether functions. At the same time, the positive regions identified in blue were located in some regions of the steroidal skeleton and associated to the methyl groups of monosaccharides. Most of the uncharged zones, green in color, are distributed throughout the molecule, which predicts an improvement in the lipophilic character of the hybrids, making them more soluble in less polar solvents.

Additionally, the dipole moments were retrieved from DFT calculation, which depends directly on the molecular geometry. It was found that the spatial arrangement of the spacer malonate carbonyl group has a high contribution to the net dipole moment of the molecule. In compound **5a**, the carbonyls are in opposite positions (-171°), so the vector of the central dipole moment practically cancels out and the molecule's dipole moment is the smallest (3.02 D). The arrangement of the carbonyl groups in **5b** is perpendicular; therefore, the maximum contribution to the net dipole moment is obtained among the analyzed compounds with a value of 7.05 D. For the remaining hybrids **5c** (5.04 D), **5d** (5.86 D), and **6** (5.38 D) the contribution of the carbonyl groups are intermediate.

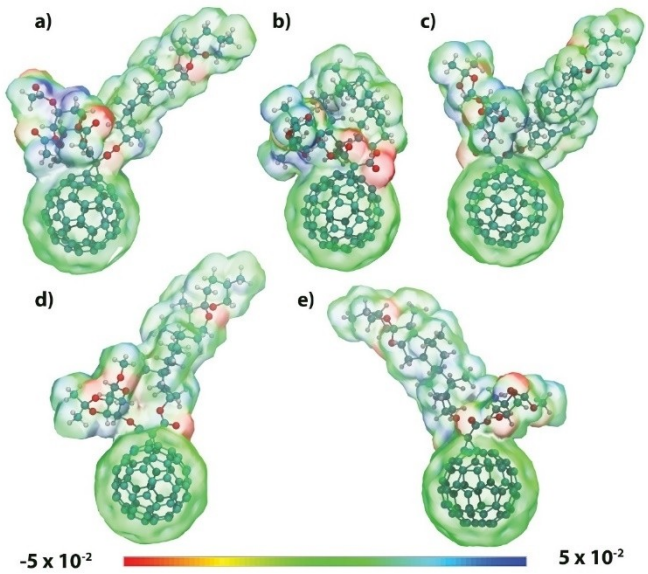


**Figure 4.** Depiction of the molecular electrostatic potential maps for the optimized structure of **5a** (a), **5b** (b), **5c** (c), **5d** (d), and **6** (e). The red color, represented negative potential, the blue color the positive potential and the green color the uncharged regions.

The electrochemical behavior of monosaccharide-steroid-methano[60]fullerene **5a**–**5d** and **6** was investigated by cyclic voltammetry using $CH_2Cl_2$ as solvent. Table 1 shows the obtained results. All the compounds exhibit two quasi-reversible fullerene-based reductions and another one or two reduction processes that are chemically irreversible (see Figure S77 and S78 in the Supporting Information), presumably due to the cleavage of one of the cyclopropane bonds connecting the addend to $C_{60}$. The cathodic shift observed in the derivatives when compared with $C_{60}$, is a consequence of the saturation of a double bond in the fullerene sphere after the formation of the monoadducts, which leads to higher energies of the LUMO and to a decrease in the electronic affinity.

For similar electrochemical results, see the previously reported information on Bingel–Hirsch-type steroid–fullerene hybrids.[22–24] The modifications on the sugar or the steroids have no effects on the reduction potentials of the Bingel-Hirsch adducts. The energy values obtained for the DFT method are close to those estimated by cyclic voltammetry with experimental deviations of ~0.03 eV. Differences in the potential values are within experimental error.

A thermogravimetric analysis (TGA) was performed to assess the thermal stability of the newly synthesized materials. Thus, TGA of the synthesized methano[60]fullerenes are represented to show that the hybrids exhibit a slight weight loss between 100 and 150 °C corresponding to the loss of solvent molecules (See Figure S79–S82 in the Supporting Information). According to the theoretical DFT calculations, it was determined that **5a** shows the HOMO with the lowest energy, to which the highest thermodynamic stability is attributed. **5a** presents the thermogram with the lowest mass loss up to 300 °C and a mass variation of 0.2 %/°C, which corresponds with the theoretical studies. Taking into account the results obtained from the thermal behavior of the hybrids, they can be considered thermally stable solids in the range of 25–100 °C. The stability in this temperature range allows its potential use for different medicinal and materials chemistry applications.

Predicting the absorption, distribution, metabolism and excretion (ADME) properties in silico of organic molecules

**Table 1.** Redox Potentials obtained in $CH_2Cl_2$ vs. Ferrocene (mV) and estimated LUMO levels (eV).[a]

| Compound | $E^1_{1/2, red}$ | $E^2_{1/2, red}$ | $E^3_{1/2, red}$ | LUMO[c] | LUMO[d] |
|---|---|---|---|---|---|
| $C_{60}$ [a] | −860 | −1440 | −2000 | −4.24 | – |
| **5a** | −1063 | −1417 | −1922 | −4.04 | −4.07 |
| **5b** | −1074 | −1475 | −2138 | −4.03 | −4.06 |
| **5c** | −1052 | −1428 | −1995 | −4.05 | −4.08 |
| **5d** | −1078 | −1446 | −2003 | −4.02 | −4.05 |
| **6** | −1049 | −1413 | −1860 | −4.05 | −4.08 |

[a] Experimental conditions: GCE as working electrode, Pt as the counter electrode, $Ag/AgNO_3$ as the reference electrode, $Bu_4N^+PF_6^-$ (0.1 M) as the supporting electrolyte, 100 mV/s scan rate. Experimental error ±5 mV.[50] [b] Cathodic peak potentials, irreversible processes. [c] LUMO = −($E^1_{1/2}$ red + 5.1).[51] [d] Calculated by DFT.

continues to play a fundamental role in drug discovery.[52] Preliminary estimates of the permeability of organic molecules can be made based on their molecular structures. The physicochemical properties examined were lipophilicity (log P), polar surface area (PSA), hydrophilicity index (Hy), and solvent-accessible surface area (SASA). Table 2 shows the results of the evaluated properties.

The *n*-octanol/water partition coefficient (log P) is a traditional molecular transport descriptor used to measure hydrophobicity or lipophilicity related to cell membrane penetration and permeability of organic molecules.[56] The log P values calculated for each compound indicate an electrostatic distribution that increases the lipophilicity of the hybrids. The higher lipophilicity value obtained for the **5 b** derivative can be attributed to the cholesterol moiety in the hybrid, which is less polar than the diosgenin. It is curious that although hybrid **6** is the only unprotected derivative with two free hydroxyl groups, it does not have the lowest log P value. The hydroxyl groups of **6** can form intramolecular hydrogen bonds, which suggests that they have little participation in the interaction with the polar molecules of the solvent. It was observed in the optimized structure in Figure 4. Although log P is a good predictor of permeability across biological membranes, lipophilicity is not the only determinant of cell permeability and other factors have been shown to affect the overall permeability of a molecule.

PSA is another property that has emerged as an estimation of permeability and has been used to predict passage through the blood-brain barrier and human intestinal absorption.[57] The topological polar surface area (TPSA) was calculated since the results are computationally faster and homologous to the classical estimation of the PSA. The literature suggests that patency is optimal when the TPSA is $<120$ Å$^2$ based on a study of commercially available drugs.[58] Only two hybrids exceed 120 Å$^2$, corresponding to the derivatives with acetate groups (**5 a**) and hydroxyl groups (**6**) in the monosaccharide units. The high TPSA values may indicate the higher desolvation energy required to overcome the strong carbonyl: water and hydroxyl: water interactions in **5 a** and **6**, respectively. It is postulated that the polar groups resist desolvation when passing from an aqueous extracellular environment to the interior of membranes. Thus, PSA measures part of the desolvation energy to break the solute: water interaction necessary for membrane transport.

**Table 2.** Theoretical physicochemical parameters calculated for the hybrids **5 a**–**5 d** and **6**.

| Property | 5 a | 5 b | 5 c | 5 d | 6 |
|---|---|---|---|---|---|
| log P[a] | 13.65 | 22.43 | 17.35 | 21.93 | 20.36 |
| TPSA (Å$^2$)[b] | 185.49 | 98.75 | 117.21 | 107.98 | 129.98 |
| Hy[c] | −6.03 | −6.24 | −6.16 | −6.17 | −6.11 |
| SASA (Å$^2$)[d] | 1305.37 | 1113.65 | 1232.75 | 1260.53 | 1229.99 |

[a] Predicted *n*-octanol/water partition coefficient (lipophilicity) using XLOGP2v3.2.0.[53] [b] Topological polar surface area calculated by BioTriangle web server.[54] [c] Hydrophilic index calculated by BioTriangle web server.[54] [d] Solvent-accessible surface area calculated by FreeSASA 2.0.3 with Lee & Richards algorithm.[55]

On the other hand, we also determined the hydrophilicity index (Hy), which predicts water solubility and follows the same trend as the TPSA. As expected, this magnitude shows the opposite results to lipophilicity. The less lipid-soluble hybrid (**5 a**) shows the highest hydrophilic behavior (−6.026), due to the possible interaction between the mannose unit and the water molecules through four carbonyl groups forming H-bonds.

The solvent-accessible surface area (SASA) is an important property that can explain intermolecular interactions and the degree of folding in a molecule. **5 b** presents the lowest SASA (1113.65 Å$^2$), due to steroid folding. Moreover, the interface between the monosaccharide and the steroid is limited to interaction with the solvent. In the case of the other hybrids, the diosgenin backbone is fully extended, allowing solvent interaction with the steroid and the monosaccharide.

Therefore, considering the results, the hybrid molecules **5 a**–**5 d** and **6**, may penetrate through lipid membranes and cross the blood-brain barrier, which would be important for possible biological applications.

The interaction of the synthesized fullerene derivatives with the main protease of SARS-CoV-2 (Mpro) was studied by analyzing the binding energy of the different complexes generated by Molecular Docking. The $C_{60}$ core interacts with the main protease of SARS-CoV-2 as reported in silico assays.[59] The active site shows a pocket shape which allows the accommodation of small ligands inside it. Moreover, Mpro has a catalytic dyad H41 and C145 involved in specific interactions with the substrates.

The docking parameters selected were corrected using the crystallization ligand (**G65**) where the best conformation has the same binding mode that in the protein PDB with an RMSD value of $<2$ Å. The ligand-Mpro complexes were grouped in clusters and the group with the highest number of solutions and the lowest average energy was selected as the representative binding mode for each fullerene derivative. Of the total number of conformations obtained, more than 90% of the conformations present a structural overlap with an RMSD value of 2 Å for each ligand (See Table S4 in the Supporting Information). Table 3 shows the affinity values for the hybrids.

All hybrids present a negative energy binding lower than that calculated for G65, showing the affinity of these derivatives for this SARS-CoV-2 receptor. Although there are no significant differences between the binding values of the hybrids, it should be noted that the rhamnose products present the highest affinities. The removal of the isopropylidene group resulted to be a method to barely increase the scoring function. The

**Table 3.** Molecular docking results of fullerene hybrids with Mpro.

| Ligand | Binding energy [kcal/mol] Cluster A | Cluster |
|---|---|---|
| **5 a** | −9.5 | −9,0 |
| **5 b** | −9.4 | −8,1 |
| **5 c** | −10.4 | −9,6 |
| **5 d** | −11.8 | −11,3 |
| **6** | −13.8 | −13,0 |
| **G65** | −9.3 | −8,7 |

Research Article
doi.org/10.1002/ejoc.202201301


amphipathic nature of the $C_{60}$-anchored malonate determined the region of the molecule for which interactions were established. All the generated conformations showed a preferential disposition of the monosaccharide fragment inside the enzyme, while the steroid was exposed on the protease surface. Representative conformations of each ligand are represented in Figure 5.

It was possible to observe polar interactions in all studied clusters. The carbonyl group of the malonate forms hydrogen bonding with N142, E166, D187, and Q189. These superficial residues bind the ligand to the interior of the receptor. In addition, the monosaccharide fragment is responsible for the interaction with the catalytic dyad. The sugar forms hydrogen bonds fundamentally through the different protective groups of the oxygen atoms. For residue H41, aromatic H-bonds with ether and carbonyl groups of the monosaccharides were observed in some clusters (Table 4).

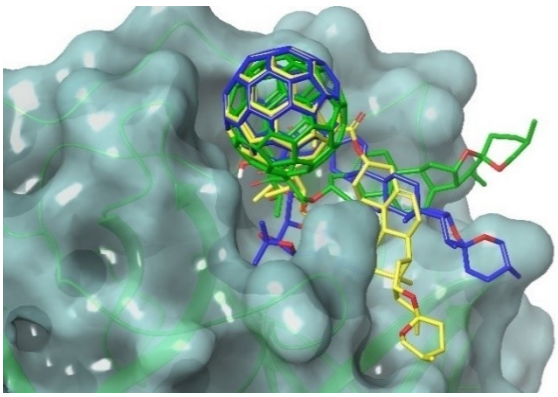

**Figure 5.** Superimposed image of hybrids-Mpro complex with the lower binding energy: **5 b** (blue), **5 d** (yellow), **6** (green).

**Table 4.** Molecular docking results of fullerene hybrids with Mpro.

| Ligand | Cluster A | Cluster |
|---|---|---|
| **5 a** | H41, N142, C145, E166 | H41, H41*, N142, C145, Q189 |
| **5 b** | H41*, C145, Q189 | H41, N142, C145, Q189 |
| **5 c** | H41*, N143, C145, E166 | H41*, C145, Q189 |
| **5 d** | H41*, Q189 | H41, N142, E166 |
| **6** | H41, N142, Q166 | H41, D187, Q189 |
| **G65** | H164, S144, C145 | L141, C145 |

*aromatic H-bonds

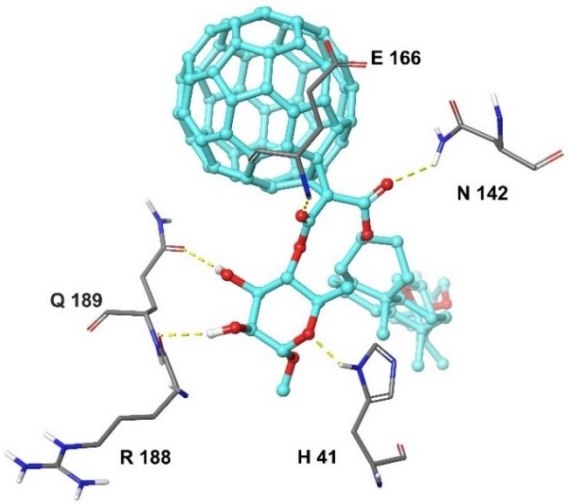


**Figure 6.** Polar interactions of **6** with Mpro residues. The H-bonds are represented in yellow discontinued lines.

In similar studies Calvaresi et al.[59a] determined that the core of $C_{60}$ occludes the enzyme cavity and interacts directly with the catalytic residue H41 by π-π stacking interactions. In our case, the interactions reported for $C_{60}$ are replaced by polar interactions of the monosaccharide in the cavity. The representative conformation for **6** is shown in Figure 6. It was observed that the free hydroxyl groups of the sugar form hydrogen bonds with the carbonyl groups of R188 and Q189, and the oxygen atom of the rhamnose ring interacts with H41. The preference of the monosaccharide for the active site leaves the fullerene core exposed on the enzyme surface and makes it a hydrophobic blocker for competing ligands.

The presence of polar groups in the monosaccharide moiety increases the hydrogen bonds formation. These results, both in energy and number of interactions, were higher than those obtained in previous work in the same computational conditions by our group for an androsterone-$H_2$@$C_{60}$ hybrid.[25]

## Conclusions

In summary, in this paper we report new hybrids using [60]fullerene as a platform, showing steroid and monosaccharide moieties in their structures by using the Bingel– Hirsch methodology. The cyclopropanation of the steroid-monosaccharide malonates with $C_{60}$ provided methano[60]fullerene derivatives (**5 a**–**5 d** and **6**). An exhaustive spectroscopic and analytical study confirmed the chemical structure of the new compounds to be unambiguously determined. Also, the proposed structures are supported by their electronic spectra and cyclic voltammetry investigations, which reveals the spectroelectrochemical features of methanofullerene monoadducts. Besides, theoretical calculations predicted the most stable conformations of the synthesized monosaccharide-steroid-fullerene derivatives, showing that hydrogen bonding plays a major role in the geometry of these hybrid molecules. The molecular docking studies suggested the possible application of these compounds as anti- SARS-CoV-2, due to their ability to inhibit the Mpro protease, the one that has a key role in the virus life cycle, notably in mediating viral replication and transcription. The calculated physicochemical parameters achieved by the presence of steroid and carbohydrate moieties in these fullerene hybrids, could contribute to enhancing the predicted activity, which is a promising result to explore further in the search for biomedical applications of these molecular systems.

## Experimental Section

**General**: All reagents were of commercial quality and were used as supplied unless otherwise specified. Solvents were dried by standard procedures. All reactions were performed using an atmosphere of argon and oven-dried glassware. Reactions were monitored by thin-layer chromatography carried out on 0.25 mm silica gel plates (230-400 mesh). Flash column chromatography was performed using silica gel (60 Å, 32–63 μm). $^1$H NMR spectra were recorded at 700 MHz, and $^{13}$C NMR at 175 MHz; the one-bond heteronuclear correlation (HMQC) and the long-range $^1$H-$^{13}$C correlation (HMBC spectra were obtained by use of the inv4gs and the inv4gslplrnd programs). HRMS were recorded under ESI and MALDI (dithranol as matrix) conditions in a positive mode of detection. Microanalysis was performed with a Perkin–Elmer 2400 CHN instrument. A high-performance liquid chromatography (HPLC) system (Cosmosil Buckyprep preparative column, dimensions, 4.6×250 mm$^2$; flow rate 1.0 mL min$^{-1}$, injection volume 15 μL, eluent toluene) was used to determine the purity of the compounds synthesized. The retention times ($t_R$) reported were determined at a wavelength of 320 nm. FTIR spectra were carried out using the ATR of the solid compounds. UV/Vis spectra were recorded in toluene. Electrochemical measurements were performed with a three-electrode configuration system. The measurements were carried out with $CH_2Cl_2$ solutions [0.1 M in tetrabutylammonium hexafluorophosphate ($TBAPF_6$)]. A glassy carbon electrode (3 mm diameter) was used as the working electrode, and a platinum wire and an $Ag/AgNO_3$ electrode were employed as the counter and the reference electrode, respectively. Ferrocene (Fc) was added as an internal reference, and all potentials were determined relative to the $Fc/Fc^+$ couple. Both the counter and the reference electrodes were directly immersed in the electrolyte solution. The surface of the working electrode was polished with commercial alumina before use. Solutions were stirred and deaerated by bubbling argon for a few minutes before each measurement. Unless otherwise specified, the scan rate was 100 mV/s and the experimental error ±5 mV. TGA analyses were carried out under air and nitrogen in a TATGA-Q500 apparatus. The sample (~0.5 mg) was introduced inside a platinum crucible and equilibrated at 90 °C followed by a 10 °C min$^{-1}$ ramp between 90 and 1000 °C.

**Computational methods**: All molecules were built with Avogadro.[60] First the structure of the molecules were optimized using semi-empirical GFN2-xTB[44][43] using xtb[61] (version 6.4) application. The optimization war run using vtight keyword to increase the accuracy of the optimization. Then those optimized structures were used as a starting point for DFT calculations which were performed with ORCA 4.2.1.[62] The gradient-corrected exchange-correlation functional of Perdew, Burke, and Ernzerhof (PBE)[47] functional was chosen for optimization and calculation of properties using first the double-zeta 6-31G(d) and then refined with 6-311G(d,p) basis set.[49] In all DFT calculations, dispersion correction was applied (D3BJ),[48] and TightOpt keyword was used to reduce numerical noise in the gradient. The frontier orbitals HOMO/LUMO were visualized directly from the optimized structure with DFT/PBE quantum mechanical calculation with 6-311G(d,p) basis set. The mep.py python script written by Marius Retegan[63] was used for cube file preparation and then molecular electrostatic map were visualized using VMD 1.9.3.[64] NCI analysis was performed using NCIPLOT 4.0[65] and the results were visualized with VMD 1.9.3. Mercury 2020.1[66] was used for the representation of optimized structures.

## Molecular Docking

*Ligand/Protein Preparation.* The structure of Mpro [PDB code: 7JU7, (R = 1.60 Å)[67] was retrieved from Protein Data Bank (PDB) (http://rcsb.org). The optimized structures of the ligands were obtained from the DFT calculations.[46] PDB files of the protease and ligands underwent a conversion to PDBQT format to perform molecular docking simulations with AutoDock Tools.[68] The Gasteiger model was used for the calculations of the partial charges of the ligands. Nonpolar hydrogen atoms were merged and default rotatable bonds were retained, except for the fullerene that was set to un-rotatable, using TORSDOF utility in AutoDock Tools. The simulation box was positioned at the center of the active site of the protease with size 30×30×30 Å$^3$.

*Simulation and Analysis of Docking Results.* Nonflexible docking simulations were performed using AutoDock Vina 1.1.2.[69] Docking parameters were set to default. Ten independent runs were performed in each case, each run's two best-docked conformations each run were analyzed, according to the affinity calculated with the scoring function. Each docking simulation produced 20 different docked conformations, which were then grouped based upon *Root Mean Square Deviation* (RMSD) of the different bound poses. The RMSD difference between conformations of the same cluster was set to less than 2 Å. The binding free energy (kcal/mol) of every cluster was calculated as the mean binding free energy of all the conformations present in the same cluster. The cluster with the best-scoring pose (higher number of conformations with the lowest mean binding energy) was used as a representative binding mode for each complex. 3D structures were represented using Schrödinger Maestro 13.2.[70]

## Synthesis and Characterization

**Synthesis of mono-carboxylic malonates 2a and 2b**: To a solution of the appropriate steroid diosgenin (**1a**) or cholesterol (**1b**) (4.82 mmol) in toluene (100 mL), Meldrum's acid (1.04 g, 7.24 mmol) was added and the mixture was stirred under reflux. After 1 h the solvent was removed under reduced pressure. The crude product was purified by column chromatography on silica gel with n-hexane/ethyl acetate (1 : 1) as the eluent.

## Synthesis of steroid-sugar conjugates

### Method A

**(22R,25R)-spirost-5-en-3β-yl malonate-2′,3′,4′,6′-tetra-O-acetyl-β-D-mannopyranoside (4a)**: A solution of malonate **2a** (0.94 g, 1.87 mmol), **3a** (0.54 g, 1.10 mmol), 4 Å molecular sieves (0.5 g) in dry $CH_2Cl_2$ (10 mL) was stirred for 5 min. The solution was cooled to 0 °C and $BF_3{\cdot}Et_2O$ (0.3 mL, 2.37 mmol) was added over 5 min over argon. The mixture was stirred for 1 h at room temperature and the reaction mixture was neutralized with $Et_3N$, filtered through Celite, the solvent was removed and the

residue was purified by column chromatography in silica gel with *n*-hexane/ethyl acetate (3 : 1) as the eluent.

**Method B**

To a stirred solution of the corresponding monosaccharide **3 b** or **3 c** (0.38 mmol) in dry $CH_2Cl_2$ (5 mL), was added the corresponding malonic acid (**2 a** or **2 b**) (0.5 mmol) followed by EDC·HCl (221 mg, 1.15 mmol). After stirring at 25 °C for 1 h the mixture was diluted with $CH_2Cl_2$ (5 mL). The solution mixture was washed with two 10 mL portions of water and saturated NaCl aqueous solution (15 mL). The organic layer was dried ($MgSO_4$) and filtered, and the solvent was removed under reduced pressure. The crude product was purified by column chromatography on silica gel with *n*-hexane/ethyl acetate (6 : 1) as the eluent.

**Synthesis of Bingel-Hirsch hybrids**: A solution of $C_{60}$ (50 mg, 0.069 mmol) in toluene (100 mL) was prepared. The corresponding malonate (0.069 mmol), $CBr_4$ (0.12 mmol), and diazabicyclo[4.2.0]undec-7-ene (DBU; 0.19 mL, 1.35 mmol) were added in that order. The reaction mixture was then stirred at room temperature for 2 h. Water was added, and the residue was extracted with toluene. The combined extracts were dried ($MgSO_4$) and filtered, and the solvent was removed under reduced pressure. Purification of the products was achieved by column chromatography on silica gel, first with $CS_2$ to elute unreacted $C_{60}$ and finally with dichloromethane for the monoadduct.

## *Acknowledgements*

*Financial support by the Spanish Ministry of Science and Innovation (projects PID2020-114653RB-I00 and PID2020-115120GB-I00), PNCB of MES, Cuba (P223LH-001-059), and Yachay Tech Internal Project (CHEM20-08) "Theoretical and Morphological studies of $C_{60}$ derivatives"*

## *Conflict of Interest*

The authors declare no conflict of interest.

## Data Availability Statement

The data that support the findings of this study are available in the supplementary material of this article.

**Keywords:** molecular docking · SARS-CoV-2 · sugar steroid hybrids · theoretical calculations · [60]Fullerene

[1] H. W. Kroto, J. R. Heath, S. C. O'Brien, R. F. Curl, R. E. Smalley, *Nature* **1985**, *318*, 162–163.
[2] a) B. Kulnitskiyac, V. Churkinac, E. Skrylevab, Y. Parkhomenkob, S. Zholudeva, V. Blankac, M. Popova, *Diamond Relat. Mater.* **2022**, *124*, 108911; b) H. Kaur, J. Kaur, R. Kumar, *Mater. Today: Proc.* **2022**, *48*, 1095–1102.
[3] M. Gaur, C. Misra, A. B. Yadav, S. Swaroop, F. Ó. Maolmhuaidh, M Bechelany, A Barhoum, *Materials* **2021**, *14*, 5978.
[4] a) E. I. Pochkaeva, N. E. Podolsky, D. N. Zakusilo, N. E. Zakusilo, D. M. Petrov, V. Andrey, N. A. Charykov, T. D. Vlasov, A. V. Penkova, L. V. Vasina, I. V. Murin, V. V. Sharoyko, *Prog. Solid State Chem.* **2020**, *57*, 100255; b) L. Tanzi, M. Terreni, Y. Zhang, *Eur. J. Med. Chem.* **2022**, *230*, 114104; c) M. Ajrin, A. Akther, *Int. J. Pharm. Sci. Res.* **2020**, *60*, 84–89.
[5] K. N. Alagarsamy, S. Mathan, W. Yan, A. Rafieerad, S. Sekaran, H. Manego, S. Dhingra, *Bioact. Mater.* **2021**, *6*, 2261–2280.
[6] V. S. Lemos, R. D. Aires, M. Ladeira, S. Guatimosim, in *Bioengineering Applications of Carbon Nanostructures* (Eds: Jorio A.), *Nanomedicine and Nanotoxicology*, Springer, Cham. **2016**, 71–84.
[7] a) T. Yasuno, T. Ohe, H. Kataoka, K. Hashimoto, Y. Ishikawa, K. Furukawa, Y. Tateishi, T. Kobayashi, K. Takahashi, S. Nakamura, T. Mashino, *Bioorg. Med. Chem. Lett.* **2021**, *31*, 127675; b) P. R. Riley, R. J. Narayan, *Curr. Opi. Biomed. Eng.* **2021**, *17*, 100262.
[8] D. A. Heredia, A. M. Durantini, J. E. Durantini, E. N. Durantini, *J. Photochem. Photobiol. C* **2022**, *51*, 100471.
[9] a) V. V. Sharoyko, O. S. Shemchuk, A. A. Meshcheriakov, L. V. Vasina, N. R. Iamalova, M. D. Luttsev, D. A. Ivanova, A. V. Petrov, D. N. Maystrenko, O. E. Molchanov, K. N. Semenov, *Nanomedicine Nanotechnology, Biol. Med.* **2022**, *40*, 102500.
[10] a) N. B. Fernandes, R. U. K. Shenoy, M. K. Kajampady, E. M. Cleona, R. K. Shirodkar, L. Kumar, R. Verma, *Environ. Sci. Pollut. Res. Int.* **2022**, *29*, 58607–58627; b) I. Gallego, J. Ramos-Soriano, A. Méndez-Ardoy, J. Cabrera-González, I. Lostalé-Seijo, B. M. Illescas, J. J. Reina, N. Martín, J. Montenegro, *Angew. Chem. Int. Ed.* **2022**, e202210043.
[11] P. Y. Xu, X. Q. Li, W. G. Chen, L. L. Deng, Y. Z. Tan, Q. Zhang, S. Y. Xie, L. S. Zheng, *Nanomaterials* **2022**, *12*, 2547.
[12] a) H. Kazemzadeh, M. Mozafari, *Drug Discovery Today* **2019**, *24*, 898–905; b) V. V. Sharoyko, S. V. Ageev, N. E. Podolsky, A. V. Petrov, E. V. Litasova, T. D. Vlasov, Timur, L. V. Vasina, I. V. Murin, L. B. Piotrovskiy, N. K. Semenov, *J. Mol. Liq.* **2021**, *323*, 114990.
[13] S. Bosi, T. Da Ros, G. Spalluto, M. Prato, *Fullerene derivatives: an attractive tool for biological applications, Eur. J. Med. Chem.* **2003**, *38*, 913–923.
[14] a) R. Caballero, P. De La Cruz, F. Langa, *RSC Nanosci. Nanotechnol.* **2012**, *20*, 66–124; b) Z. Q. Liu, *Curr. Org. Synth.* **2017**, *14*, 999–1021; c) A. Hirsch, M. Brettreich, *Fullerenes. Chemistry and Reactions*, Wiley-VCH Verlag GmbH & Co. KGaA, Weinheim, **2005**.
[15] a) C. Bingel, *Chem. Ber.* **1996**, *26*, 1957–1959; b) Y. N. Biglova, *Beilstein J. Org. Chem.* **2021**, *17*, 630–670.
[16] Y. N. Biglova, A. G. Mustafin, *RSC Adv.* **2019**, *9*, 22428–22498.
[17] X. Camps, A. Hirsch, *J. Chem. Soc.* **1997**, 1595–1596.
[18] R. Kessinger, M. Gómez-López, C. Boudon, J.-P. Gisselbrecht, M. Gross, L. Echegoyen, F. Diederich *J. Am. Chem. Soc.* **1998**, *120*, 8545–8546.
[19] a) M. Maggini, G. Scorrano, M. Prato, *J. Am. Chem. Soc.* **1993**, *115*, 9798–9799; b) M. Prato, M. Maggini, *Acc. Chem. Res.* **1998**, *31*, 519–526.
[20] M. Suárez, Y. Verdecia, B. Illescas, R. Martínez-Alvarez, A. Alvarez, E. Ochoa, C. Seoane, N. Kayali, N. Martín, *Tetrahedron* **2003**, *59*, 9179–9186.
[21] a) D. Alonso, D. Hernandez-Castillo, L. Almagro, R. Gonzalez-Aleman, D. Molero, M. Á. Herranz, E. Medina-Paez, J. Coro, R. Martinez-Alvarez, M. Suarez, N. Martín, *J. Org. Chem.* **2020**, *85*, 2426–2437.
[22] J. Coro, H. Rodríguez, D. G. Rivera, M. Suárez, D. Molero, M. Á. Herranz, R. Martínez-Alvarez, S. Filippone, N. Martín, *Eur. J. Org. Chem.* **2009**, *2009*, 4810–4817.
[23] L. Almagro, D. Hernández-Castillo, O. Ortiz, D. Alonso, A. Ruiz, J. Coro, M. Á. Herranz, D. Molero, R. Martínez-Álvarez, M. Suárez, N. Martín, *Eur. J. Org. Chem.* **2018**, *2018*, 4512–4522.
[24] L. Almagro, R. Lemos, K. Makowski, H. Rodríguez, O. Ortiz, W. Cáceres, M. Á. Herranz, D. Molero, R. Martínez-Álvarez, M. Suárez, N. Martín, *Eur. J. Org. Chem.* **2020**, *2020*, 5926–5937.
[25] M. Suarez, K. Makowski, R. Lemos, L. Almagro, M. Á. Herranz, D. Molero, H. Rodriguez, F. Albericio, Y. Murata, N. Martín, *ChemPlusChem.* **2021**, *86*, 972–98.
[26] A. K. Ghosh, K. V. Rao, P. R. Nyalapatla, H. L. Osswald, C. D. Martyr, M. Aoki, H. Hayashi, J. Agniswamy, Y. F. Wang, H. Bulut, D. Das, I. T. Weber, H. Mitsuya, *J. Med. Chem.* **2017**, *60*, 4267–4278.
[27] Y. M. Báez-Santos, S. J. Barraza, M. W. Wilson, M. P. Agius, A. M. Mielech, N. M. Davis, S. C. Baker, S. D. Larsen, A. D. Mesecar, *J. Med. Chem.* **2014**, *57*, 2393–2412.

[28] Z. Jin, X. Du, Y. Xu, Y. Deng, M. Liu, Y. Zhao, B. Zhang, X. Li, L. Zhang, C. Peng, Y. Duan, J. Yu, L. Wang, K. Yang, F. Liu, R. Jiang, X. Yang, T. You, X. Liu, X. Yang, F. Bai, H. Liu, X. Liu, L. W. Guddat, W. Xu, G. Xiao, C. Qin, Z. Shi, H. Jiang, Z. Rao, H. Yang, *Nature* **2020**, *582*, 289–293.
[29] R. Lemos, F. Ortiz, L. Almagro, K. Makowski, N. Martin, F. Albericio, M. Suárez, H. Rodríguez, *Surf. Interface Anal.* **2022**, *54*, 1041–1051.
[30] M. Ibrahim-Ouali, F. Dumur, *Arkivoc* **2022**, 140–164.
[31] M. E. Ragoussi, S. Casado, R. Ribeiro-Viana, G. de la Torre, J. Rojo, T. Torres, *Chem. Sci.* **2013**, *4*, 4035–4041.
[32] T. Mashino, *J. Pharm. Soc. Jpn.* **2022**, *142*, 165–179.
[33] a) A. Muñoz, D. Sigwalt, B. M. Illescas, J. Luczkowiak, L. Rodríguez-Pérez, I. Nierengarten, M. Holler, J. S. Remy, K. Buffet, S. P. Vincent, J. Rojo, R. Delgado, J. F. Nierengarten, N. Martín, *Nat. Chem.* **2015**, *8*, 50–57; b) J. Ramos-Soriano, B. M. Illescas, A. Pérez-Sánchez, R. Sánchez-Bento, F. Lasala, J. Rojo, R. Delgado, N. Martín, *Int. J. Mol. Sci.* **2022**, *23*, 5083.
[34] S. Tanimoto, S. Sakai, E. Kudo, S. Okada, S. Matsumura, D. Takahashi, K. Toshima, *Chem. Asian J.* **2012**, *7*, 911–914.
[35] J. Ramos-Soriano, M. Ghirardello, M. C. Galan, *Curr. Med. Chem.* **2022**, *29*, 1232–1257.
[36] R. Fan, W. He, Y. Fan, W. Xu, W. Xu, G. Yan, S. Xu, *Steroids* **2022**, *180*, 108991.
[37] a) R. R. Schmidt, J. Michel, *Angew. Chem. Int. Ed. Engl.* **1980**, *19*, 731–732; b) R. I. Duclos, Jr. *Carbohydr. Res.* **2000**, *328*, 489–507.
[38] a) T. Murase, H. Ishida, M. Kiso, A. Hasegawa, *Carbohydr. Res.* **1989**, *188*, 71–80; b) A. Hasegawa, N. Suzuki, F. Kozawa, H. Ishida, M. Kiso, *J. Carbohydr. Chem.* **1996**, *15*, 639–648.
[39] C. Du, J. Xu, Y. Li, W. Xu, D. Zhu, *Chin. Sci. Bull.* **2001**, *46*, 1156–1159.
[40] A. Bianco, M. Maggini, G. Scorrano, C. Toniolo, G. Marconi, C. Villani, M. Prato, *J. Am. Chem. Soc.* **1996**, *118*, 4072–4080.
[41] W. Zhou, X. Liu, L. Ye, M. Feng, P. Zhou, X. Shi, *Process Biochemistry* **2014**, *49 (9)*, 1464–1471.
[42] R. F. Enes, A. C. Tomé, J. A. S. S. Cavaliero, A. El-Agamey, D. J. McGravey, *Tetrahedron* **2005**, *61*, 11873–11881.
[43] S. Spicher, S. Grimme, *Angew. Chem. Int. Ed.* **2020**, *59*, 15665–15673; *Angew. Chem.* **2020**, *132*, 15795–15803.
[44] a) C. Bannwarth, S. Ehlert, S. Grimme, *J. Chem. Theory Comput.* **2019**, *15*, 1652–1671; b) M. Bursch, H. Neugebauer, S. Grimme, *Angew. Chem. Int. Ed.* **2019**, *58*, 11078–11087; *Angew. Chem.* **2019**, *131*, 11195–11204.
[45] C. Sikorska, T. Puzyn, *Nanotechnology* **2015**, *26*, 455702.
[46] G. L. Stoychev, A. A. Auer, F. Neese, *J. Chem. Theory Comput.* **2018**, *14*, 4756–4771.
[47] J. P. Perdew, K. Burke, M. Ernzerhof, *Phys. Rev. Lett.* **1997**, *78*, 1396.
[48] S. Grimme, S. Ehrlich, L. Goerigk, *J. Comput. Chem.* **2011**, *32*, 1456–1465.
[49] H. Wang, Y. He, Y. Li, H. Su, *J. Phys. Chem. A* **2012**, *116*, 255–262.
[50] S. A. Lerke, B. A. Parkinson, D. H. Evans, P. J. Fagan, *J. Am. Chem. Soc.* **1992**, *114*, 7807–7813.
[51] C. M. Cardona, W. Li, A. E. Kaifer, D. Stockdale, G. C. Bazan, *Adv. Mater.* **2011**, *23*, 2367–2371.
[52] M. P. Gleeson, A. Hersey, S. Hannonghbua, *Curr. Top. Med. Chem.* **2011**, *11(4)*, 358–381.
[53] T. Cheng, Y. Zhao, X. Li, F. Lin, Y. Xu, X. Zhang, Y. Li, R. Wang, L. Lai, *J. Chem. Inf. Model.* **2007**, *47*, 2140–2148.
[54] J. Dong, Z.-J. Yao, M. Wen, M.-F. Zhu, N.-N. Wang, H.-Y. Miao, A.-P. Lu, W.-B. Zeng, D.-S. Cao, *J. Cheminf.* **2016**, *8*, 34.
[55] S. Mitternacht, *F1000Research* **2016**, *5*, 189.
[56] C. A. Lipinski, F. Lombardo, B. W. Dominy, P. J. Feeney, *Adv. Drug Delivery Rev.* **2012**, *64*, 4–17.
[57] Y. H. Zhao, M. Abraham, A. Ibrahim, P. V. Fish, S. Cole, M. L. Lewos, M. J. de Goot, D. P. Reynolds, *J. Chem. Inf. Model.* **2007**, *1*, 170–175.
[58] P. Mohanty, S. Bhatnagar, *Assay Drug Dev. Technol.* **2019**, *17*, 58–67.
[59] a) T. D. Marforio, E. J. Mattioli, F. Zerbetto, M. Calvaresi, *Molecules* **2022**, *27*, 1916; b) V. V. Hurmach, M. O. Platonov, S. V. Prylutska, P. Scharff, Y. I. Prylutskyy, U. Ritter, *Sci. Rep.* **2021**, *11*, 17748.
[60] M. D. Hanwell, D. E. Curtis, D. C. Lonie, T. Vandermeersch, E. Zurek, G. R. Hutchison, *J. Cheminf.* **2012**, *4*, 17.
[61] C. Bannwarth, E. Caldeweyher, S. Ehlert, A. Hansen, P. Pracht, J. Seibert, S. Spicher, S. Grimme, *WIREs Comput. Mol. Sci.* **2020**, *11*, e01493.
[62] F. Neese, F. Wennmohs, U. Becker, C. Riplinger, *J. Chem. Phys.* **2020**, *152*, 224108.
[63] M. Retegan, *Mep.Py.* **2019**, https://gist.github.com/mretegan/5501553#file-mep-py.
[64] W. Humphrey, A. Dalke, K. Schulten, *J. Mol. Graphics* **1996**, *14*, 33–38.
[65] R. Boto, F. Peccati, R. Laplaza, A. Carbone, C. Quan, J.-P. Piquemal, Y. Maday, J. Contreras-García, *J. Chem. Theory Comput.* **2020**, *16*, 4150–4158.
[66] C. F. Macrae, I. Sovago, S. J. Cottrell, P. T. A. Galek, P. McCabe, E. Pidcock, M. Platings, G. P. Shields, J. S. Stevens, M. Towler, P. A. Wood, *J. Appl. Crystallogr.* **2020**, *53*, 226–235.
[67] N. Drayman, J. K. DeMarco, K. A. Jones, S. A. Azizi, H. M. Froggatt, K. Tan, N. I. Maltseva, S. Chen, V. Nicolaescu, S. Dvorkin, K. Furlong, R. S. Kathayat, M. R. Firpo, V. Mastrodomenico, E. A. Bruce, M. M. Schmidt, R. Jedrzejczak, M. A. Munoz-Alia, B. Schuster, V. Nair, K. Y. Han, A. O'Brien, A. Tomatsidou, B. Meyer, M. Vignuzzi, D. Missiakas, J. W. Botten, C. B. Brooke, H. Lee, S. C. Baker, B. C. Mounce, N. S. Heaton, W. E. Severson, K. E. Palmer, B. C. Dickinson, A. Joachimiak, G. Randall, S. Tay, *Science* **2021**, *373*, 931–936.
[68] M. F. Sanner, *J. Mol. Graphics* **1999**, *17*, 57–61.
[69] O. Trott, A. J. Olson, *J. Comput. Chem.* **2010**, *31*, 455–461.
[70] L. L. C. Schrodinger, Schrödinger Maestro 13.2. The PyMOL Molecular Graphics System, Version 2.1.0, **2022**.

Manuscript received: November 4, 2022
Revised manuscript received: December 21, 2022
Accepted manuscript online: December 26, 2022

# RESEARCH ARTICLE

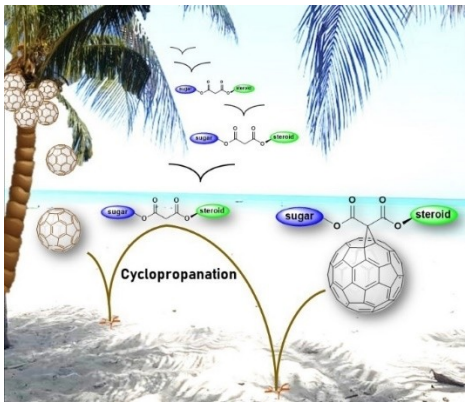


*R. Lemos, Dr. K. Makowski, Dr. L. Almagro, Dr. B. Tolón, Dr. H. Rodríguez, Dr. M. Á. Herranz, Dr. D. Molero, Prof. Dr. N. Martín*, Prof. Dr. M. Suárez**

1 – 13

**Synthesis of [60]Fullerene Hybrids Endowed with Steroids and Monosaccharides: Theoretical Underpinning as Promising anti-SARS-CoV-2 Agents**

New [60]fullerene hybrids endowed with steroid and monosaccharide moieties are obtained through a cyclopropanation reaction. The structure of monoadducts were determined by spectroscopic and analytical study. Theoretical calculations predicted the most stable conformations and determine the factors that control the hybrid molecules' geometry. The molecular docking studies suggested the possible application of these compounds as anti-SARS-CoV-2.